



## Photodetector for visible light based on Fe(phen)<sub>2</sub>(SCN)<sub>2</sub> molecule

Hayder Fahim<sup>1,2</sup>Hashim Jabbar<sup>1</sup>Adil A. Al-Fregi<sup>1</sup><sup>1</sup>University of Basrah, College of Science, Iraq/Basrah<sup>2</sup>Kerbala University, College of Education for Pure Science, Iraq/kerbala\*Corresponding Author E-mail: [hyder.fahem@uokerbala.edu.iq](mailto:hyder.fahem@uokerbala.edu.iq)

### ARTICLE INF.

#### Article history:

Received: 26 NOV., 2023

Revised: 15 MAY., 2024

Accepted: 29 MAY., 2024

Available Online: 30 JUN., 2024

#### Keywords:

Photodetector (PD)

Fe (phen),

Phen:(1,10-phenanthroline)

Photosensitivity

### ABSTRACT

This paper describes a unique method that uses Iron (phen) molecule [phen: 1,10-phenanthroline] placed on a glass substrate to create a photodetector (PD) that is sensitive to visible light as a structural, morphological, and optical heterostructure device. The properties of the samples were investigated using techniques such as X-ray diffraction (XRD), energy dispersive X-ray spectra (EDX), field emission scanning electron microscopy (FESEM), and UV-Vis spectrophotometry. The photosensitivity of the *Iron (phen) /glass* PD was evaluated at different bias voltages (5, 10, 15, and 20 V) at wavelength of 510 nm. The photosensitivity values were found to be 58.45, 76.82, 84.9, and 87.83, indicating the PD's ability to generate a measurable electrical response to light stimuli in the visible range. Furthermore, the response and recovery times of the *Iron (phen)* PD were assessed when exposed to pulsed visible light at a wavelength of 510 nm and bias voltages of 5, 10, 15 and 20 V. The results indicated favorable response and recovery times, suggesting the PD's capability to quickly detect and recover from changes in light intensity. At a bias voltage of 20 V and under illumination with visible light at 510 nm, the *Iron (phen)* PD demonstrated a maximum current gain of 9.22 and a quantum efficiency ( $\eta$ ) of 28.17. These values indicate the PD's ability to amplify the generated electrical current and efficiently convert incident photons into detectable electrical signals. Overall, the fabricated *Iron (phen)* glass PD exhibited promising photosensitivity, response and recovery times, current gain, and quantum efficiency when exposed to visible light. The findings suggest the potential application of *Iron (phen)* as a material for visible light photodetection.

DOI: <https://doi.org/10.31257/2018/JKP/2024/v16.i01.14199>

## كاشف ضوئي للضوء المرئي يعتمد على جزيء ثيوسينات الايرون فينانترولين

عادل الفرجي<sup>1</sup>هاشم جبار<sup>1</sup>حيدر فاهم<sup>1,2</sup><sup>1</sup>جامعة البصرة, كلية العلوم, العراق/بصرة<sup>2</sup>جامعة كربلاء, كلية التربية للعلوم الصرفة, العراق/كربلاء

## الخلاصة

## الكلمات المفتاحية:

كاشف ضوئي  
الحديد(فينانثرولين)  
Phen:(1,10phenanthroline)  
حساسية الضوء

تصف هذه الورقة طريقة فريدة تستخدم جزيء الحديد (فين) [فين: 10، 1-فينانثرولين] الموضوع على ركيزة زجاجية لإنشاء كاشف ضوئي (PD) حساس للضوء المرئي كجهاز ذو بنية متغايرة. تم فحص الخصائص الهيكلية والمورفولوجية والبصرية للعينات باستخدام تقنيات مثل حيود الأشعة السينية (XRD)، وأطياف الأشعة السينية المشتتة من الطاقة (EDX)، والمجهر الإلكتروني لمسح انبعاث المجال (FESEM)، والقياس الطيفي للأشعة فوق البنفسجية. تم تقييم الحساسية الضوئية للحديد (فين) / الزجاج PD عند جهود متحيزة مختلفة (5، 10، 15، و 20 فولت) عند طول موجة قدره 510 نانومتر. تم العثور على قيم الحساسية للضوء لتكون 58.45، 76.82، 84.9، و 87.83، مما يشير إلى قدرة PD على توليد استجابة كهربائية قابلة للقياس لمحفزات الضوء في النطاق المرئي. علاوة على ذلك، تم تقييم أوقات الاستجابة والاسترداد لـ Iron (phen) PD عند تعريضها للضوء المرئي النبضي عند طول موجة يبلغ 510 نانومتر وفولتية متحيزة تبلغ 5 و 10 و 15 و 20 فولت. أشارت النتائج إلى أوقات استجابة واسترداد مواتية، مما يشير إلى قدرة PD على اكتشاف التغيرات في شدة الضوء والتعافي منها بسرعة. عند جهد متحيز قدره 20 فولت وتحت الإضاءة بالضوء المرئي عند 510 نانومتر، أظهر Iron (phen) PD أقصى كسب تيار قدره 9.22 وكفاءة كمية ( $\eta$ ) قدرها 28.17. تشير هذه القيم إلى قدرة PD على تضخيم التيار الكهربائي المتولد وتحويل الفوتونات الساقطة بكفاءة إلى إشارات كهربائية يمكن اكتشافها بشكل عام، أظهر زجاج الحديد (فين) المُصنَّع حساسية ضوئية واعدة، وأوقات استجابة واسترداد، والكسب الحالي، والكفاءة الكمومية عند تعرضه للضوء المرئي. تشير النتائج إلى التطبيق المحتمل للحديد (الفين) كمادة للكشف الضوئي للضوء المرئي.

## 1 – INTRODUCTION

*Iron(phen)(SCN)* also known as (1,10 phenanthroline) (thiocyanato) iron (II), is a coordination compound that has garnered attention for its photodetection properties within the visible light range. This compound exhibits a high capacity for absorbing visible light, rendering it suitability for photodetector applications operating in this spectral region[1]. Visible light encompasses wavelengths ranging from approximately 400 to 700 nanometers, corresponding to different colors in the electromagnetic spectrum. The Iron (phen) possesses the ability to absorb visible light due to the presence of phen ligands, which act as chromophores[2]. When Iron (phen) absorbs visible light, electronic transitions occur within the molecule, causing it to transit from its ground state to an excited state[3]. Upon absorption of visible light, the *Iron*

(*phen*) can undergo various relaxation mechanisms. One possible outcome is the emission of fluorescence, whereby the molecule releases the absorbed energy in the form of light at longer wavelengths[4]. The fluorescence emission characteristics of *Iron (phen)* are reliant upon factors such as molecular structure, surrounding environment, and energy levels of the excited states. Furthermore, *Iron (phen)* can undergo nonradiative relaxation processes, where the absorbed energy dissipates as heat within the molecule[5]. This heat generation can be improved in specific applications like photothermal therapy or heat-assisted catalysis[6].

In the context of photodetection, the *Iron (phen)* can be integrated into a photodetector device to convert absorbed visible light into an electrical signal. When it absorbs visible light, charge separation occurs, leading to

the creation of an electron and a corresponding positive charge (hole) within the molecule[7]. These charges can be separated and collected by appropriate electrode systems, generating an electrical current or voltage that indicates the presence of visible light[8]. The performance of *Iron (phen)*-based photodetectors within the visible light range depends on several factors, including absorption efficiency, charge carrier mobility, response time, and device architecture[9]. Researchers have been exploring strategies to optimize these properties through molecular engineering, interface engineering, and device optimization. *Iron (phen)*-based photodetectors within the visible light range hold potential applications in areas such as optical communication, imaging, light sensing, and optoelectronic devices. Their tunable absorption properties, high sensitivity, and compatibility with existing fabrication techniques make them attractive for integration into various photonic and electronic systems[10]. It is important to note that the specific performance characteristics and efficiency of *Iron (phen)*-based photodetectors in the visible light range may vary depending on factors such as device design, film morphology, and environmental conditions. Therefore, experimental characterization and optimization are crucial for achieving the desired photodetection performance within the visible light region[11].

The present paper comes up with the discoveries in the Fabrication of *Iron (phen)* for the applications of

photodetection. It probes into the visible light area, uses nanostructured elements, studies the influence of the stimuli, and creates a flexible device architecture. The inclusions of emerging and new factors set the research apart from the recently developed and old research, bringing the modern and successful *Iron (phen)*-based photodetectors.

## 2. Experimental part

### 2.1 Preparation of bis (phenanthroline) dithiocyanato iron (II) $\text{Fe(Phen)}_2(\text{SCN})_2$

A solution (0.468 g, 2 Milli-mole) of 1,10-phenanthroline hydrochloride monohydrate, in 20 ml of distilled water was added drop by drop to an aqueous solution of (0.278 g, 1 Milli-mole), ferrous sulfate heptahydrate, in 15 ml of distilled water with gentle stirring. The mixture was stirred at room temperature for 3 hours. Then, a solution 0.152 g, 2 Milli-mole) of ammonium thiocyanate,  $\text{NH}_4\text{SCN}$ , was added. The reaction mixture was stirred to 3 hours to obtain a dark red color participate which then collected by filtration. The crude solid was washed several times with distilled water and ethanol to obtain red crystals of bis (phenanthroline) dithiocyanato iron (II) *Iron (phen)(SCN)* in 89% yield.

### 2.2 Layer of thin films of phenanthroline molecular using spin-coating:

- 1- *Iron (phen)* was dissolved in ethanol to make a concentration of 0.1-1.0 mM.

- 2- The substrate was cleaned using ultrasonication for 10 min, Acetone, Ethanol, and N<sub>2</sub> gun.
- 3- The solution was dropped onto the substrate, during rotation at 2000-4000 rpm for 30-60 s.

The samples were dried under vacuum for 1–2 h to evaporate the solvent and to form a uniform thin film[12].

### 3 Results and discussion

#### 3.1 Crystal structure analysis

XRD phase formation investigation was performed using an XPERT-PRO X-ray diffractometer with Cu-K $\alpha$  radiation ( $\lambda = 1.54 \text{ \AA}$ ) over the range  $2\theta \sim 10\text{-}80^\circ$  with a step size of  $0.02^\circ$ . The results of X-ray diffraction of iron (phen) were shown the crystal structure revealed by XRD of the SCO sample at room temperature. Phase, crystalline structure, and crystallite size were identified for a thin film form of the sample.

In Figure 1(a,b), the X-ray diffraction (XRD) pattern and surface morphology images of the thin film made of *Iron (phen)* are presented. The XRD spectrum, specifically represented in Table 1, the average crystallite size determined by XRD is 33.16 nm. The diffraction peaks positions ( $2\theta^\circ$ ) associated with the XRD pattern are presented in (Table 1).

#### 3.2 Surface morphology

The surface morphology of Iron (phen) was examined using FESEM images. Additionally, the EDX

spectrum analysis revealed peaks corresponding to elements such as Al, Fe, C, and N. The presence of Al can be attributed to the glass substrate used in the study.

Surface morphology and topography are significant characteristics of molecular materials, ranging from the nano- to the macroscale. These properties are influenced by the chemical nature/structure and production processes of the materials. The surface morphology of molecular materials plays a crucial role in determining their final surface properties, including wettability (refers to the ability of a liquid to spread over or make contact with a solid surface) and adhesiveness, which effect the light absorption and scattering. From the SEM image, it is clearly observed that the *Iron (phen)* thin film sample shows rough surface with aggregation of large number of globules that amassed over the gathered particle surfaces forming irregular grains mostly in the range of mesoscopic (refers to an intermediate size scale between the microscopic (atomic or molecular) and macroscopic (visible to the naked eye) scales) length scale. The irregular shape of the constituents might be resulted from the different mechanisms lead to (the irregular shape of the constituents in the Iron (phen) thin film sample may be a result of different mechanisms that cause the agglomeration of smaller particles. These mechanisms can be influenced by surface energies and chemical composition, which are common in organic compounds) agglomerations of smaller particle-like

caused by surface energies and chemical composition on the surface of these components of the thin film sample which is common in many organic compounds.

EDX investigation was performed to confirm the presence of Iron (Fe), Carbon (C), Nitrogen (N), and Oxygen (O), to look at the binding energies, chemical composition of the thin film structures. The acquired EDX grouping of nanoparticles is outlined in Figure 1c which demonstrate the characteristic signals for the components of Fe, C, N, and O. In common, the weight rates Fe, C, N, and O were determined from EDS for the three structures. The peaks at binding energies of 0.5, 6.45, and 7.1 keV correspond to FeL $\alpha$ , FeK $\alpha$ , and FeK $\beta$ , respectively, while the value of approximately 0.4 and 0.2 keV corresponds to the binding energies of oxygen (O-K $\alpha$ ) and (C-K $\alpha$ ). This finding confirms that the prepared sample structure consisted of Fe, C, N, and native oxides with small amount of reaction residuals or impurities.

### 3.3 Optical properties

Figure 2(a and b) illustrates the absorption and transmission spectra of a thin film composed of Iron (phen). The film's absorption spectrum displays a pronounced and intense absorbance in the ultraviolet (UV) region, specifically within the wavelength range of 300 to 900 nm. In turn, the transparency of the optical transmission in a visible range of the spectrum of the film is relatively high. The primary cause of the film's absorption can be attributed to

permitted direct transitions, which are described by the widely recognized relationship[13] [14]:

$$\alpha h\nu = A_{\alpha}(h\nu - E_g)^{1/2} \dots (1)$$

where  $\alpha$  represents the absorption coefficient,  $h\nu$  denotes the incident photon energy,  $E_g$  signifies the energy bandgap, and  $A_{\alpha}$  is a characteristic parameter that remains constant for the respective transitions, regardless of the photon energy. By plotting  $(\alpha h\nu)^2$  against  $h\nu$ , as depicted in Figure 2(c), the value of  $E_g$  was determined to be 3.2 eV (an imaging sensor with a large energy gap is an optimal Photosensitizer as it tends to result in efficient light absorption with minimal energy losses, enhanced photostability, and selective excitation.). Notably, this value closely aligns with previously reported findings[15][16].

### 3.4. Photodetector characteristics

Current-voltage (I-V) and photoresponse properties were measured by Keithley-2430 source meter and Fluke-8808 DMM respectively, connected to PC for data analysis using Visible wavelength of 510 nm illumination.

Figure 3(a) exhibits the current-voltage (I-V) characteristics of the Iron (phen) photodetector (PD) in two conditions: in the dark and under visible illumination at a wavelength of 510 nm and intensity of 33  $\mu\text{W}/\text{cm}^2$ . The curve demonstrates ohmic behavior, suggesting a favorable contact between the Iron (phen) material and the electrodes. To explore the impact of bias voltage on the photocurrent behavior ( $I_{ph}$ ) of the Iron

(phen) PD, the relationship between  $I_{ph}$  and interval time ( $I - t$ ) was depicted in Figure 3(b) at different voltages under alternating ON/OFF visible light illumination at 510 nm. It is evident that increasing the bias voltage leads to higher photocurrent values, which can be attributed to an increase in carrier diffusion velocity ( $v$ ). The carrier's mobility and electrode separation  $I$ , this velocity is a product of bias voltage  $V$  and given as ( $v = \mu V / I$ ) [17]. Additionally, the carrier's transit time ( $T_t$ ) decreases with increasing bias voltage (e.g.,  $T_t = I^2 / \mu V$ ) [17]. The levels of dark current ( $I_{dark}$ ) and photocurrent ( $I_{ph}$ ) remain stable without deviation, even after multiple cycles. Figures 3(c), (d), (e), and (f) illustrate the ( $I - t$ ) curves at bias voltages of 5 V, 10 V, 15 V, and 20 V, respectively, under various ON/OFF visible light illuminations (510 nm,  $33 \mu W/cm^2$ ). It could be noted that, after several cycles, the value of the peak photocurrent remains stable at all bias voltages, thus, indicating good stability and high reproducibility in the flexible PD. The photosensitivity  $S_{ph}$  was then calculated using the following relationship [18][19]:

$$S_{ph}(\%) = \left( \frac{I_{ph} - I_{dark}}{I_{dark}} \right) \times 100 \dots\dots (2)$$

Quantum efficiency  $\eta$  following relation is [20]:

$$\eta(\%) = \left[ \frac{I_{ph} h\nu}{q P_{in}} \right] \times 100 \dots\dots\dots (3)$$

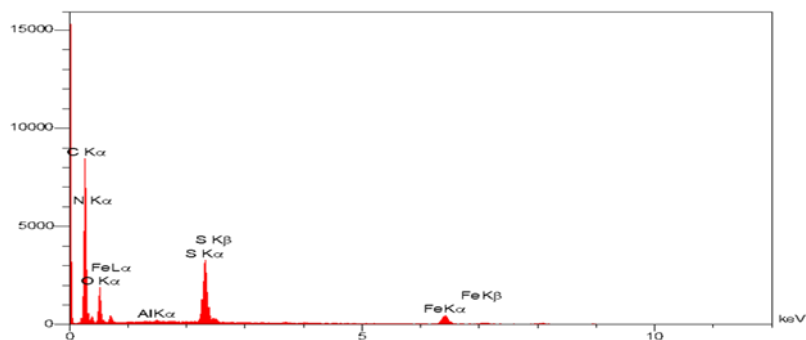
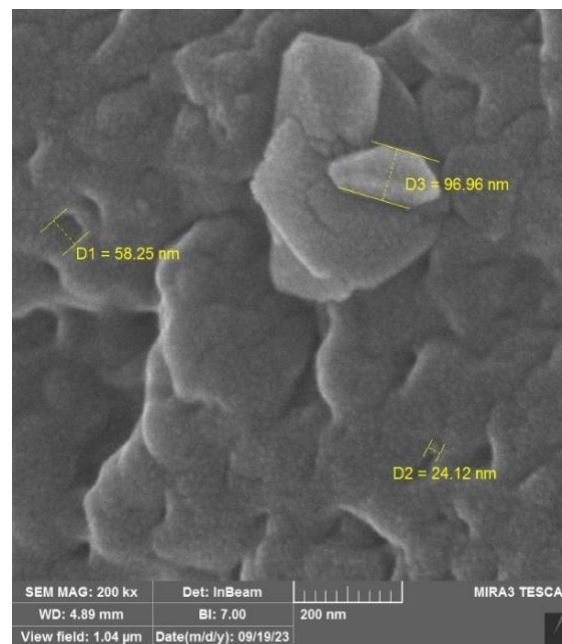
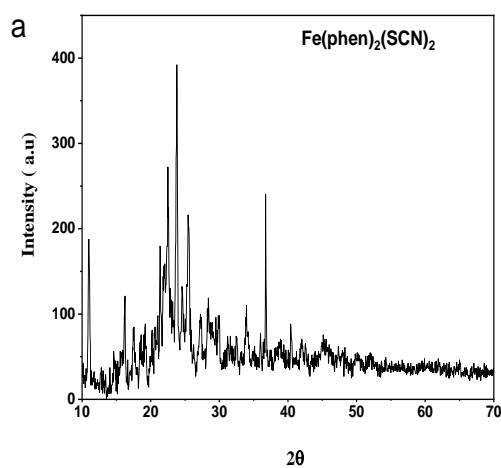
where  $P_{in}$  represents the incident power,  $h$  is the Planck constant,  $q$  is the electric charge, and  $\nu$  is the frequency of the incident light. The

values of ( $I_{ph}$ ), ( $I_{dark}$ ),  $S_{ph}$ , and gain were calculated based on Figures 3(d-g) and equations (2) and (3), and are listed in Table 2. At bias voltages of 5, 10, 15, and 20 V, the photosensitivity values for visible light (510 nm) were found to be 58.45, 76.82, 84.9, and 87.83, respectively. Notably, increasing the bias voltage resulted in higher  $S_{ph}$  values for the visible wavelength[21].

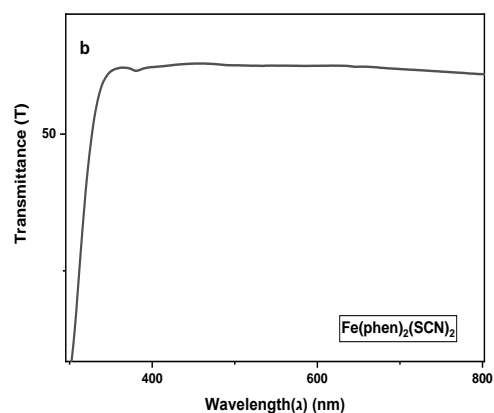
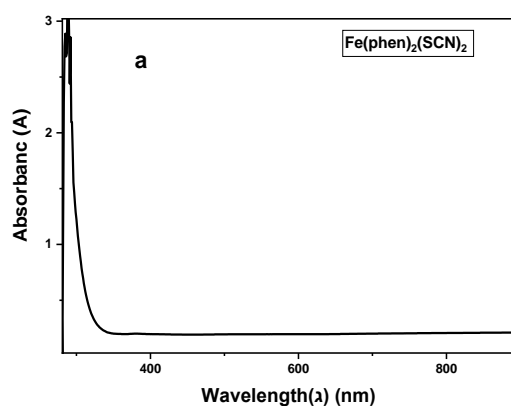
The PD exhibited a maximum current gain of 87.83 (by using the Scherrer equation: This  $\tau = (K * \lambda) / (\beta * \cos(\theta))$  where  $\tau$  is the particle size) under visible light at 510 nm and a bias voltage of 20 V, as determined from the ( $I - t$ ) characteristics. The quantum efficiency ( $\eta$ ), listed in Table 2, also increased with increasing bias voltage and reached a maximum value of 28.17 under visible illumination at 510 nm and a bias voltage of 20 V. This maximum value was achieved due to the higher photocurrent observed at 20 V compared to 5, 10, and 15 V. The response time ( $\tau_{Rec}$ ) and recovery time ( $\tau_{Rec}$ ) were calculated based on Figures 3(c-f). For visible light at 510 nm, the PD exhibited a response time of 24, 22.77, 22.73, and 14.5 seconds, and a recovery time of 45, 38.3, 41.8, and 34.5 seconds at bias voltages of 5, 10, 15, and 20 V, respectively (as shown in Table 2).

The superior optical sensitivity and quantum efficiency in the near-visible region are what advances the practical applications that require the detection of visible wavelengths. The more significant intensity of ultraviolet radiation absorption may relate to the

molecular structure and electronic features of the same as they are in close harmony with the ultraviolet photons' energy level.



**Figure 1:** Shows (a) XRD pattern, (b) FESEM image and (c) EDS spectrum of the the  $\text{Fe(phen)}_2(\text{SCN})_2$  sample.



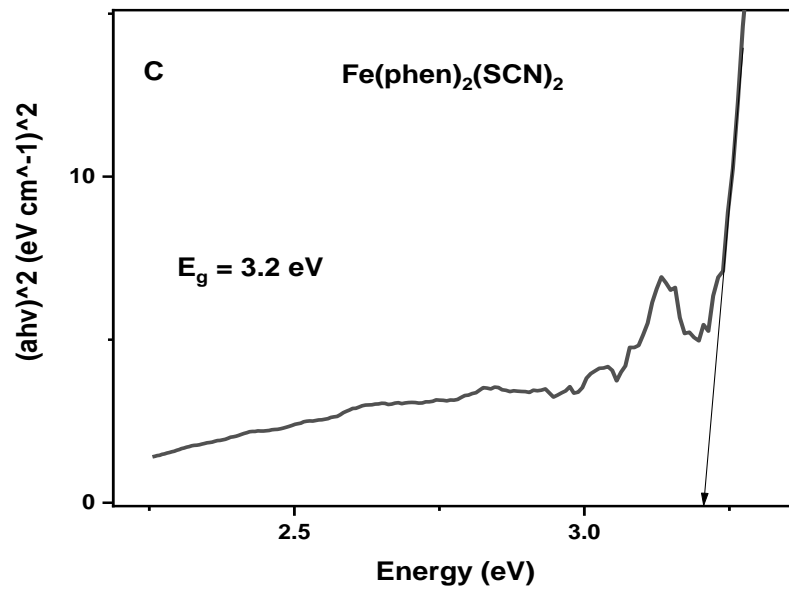
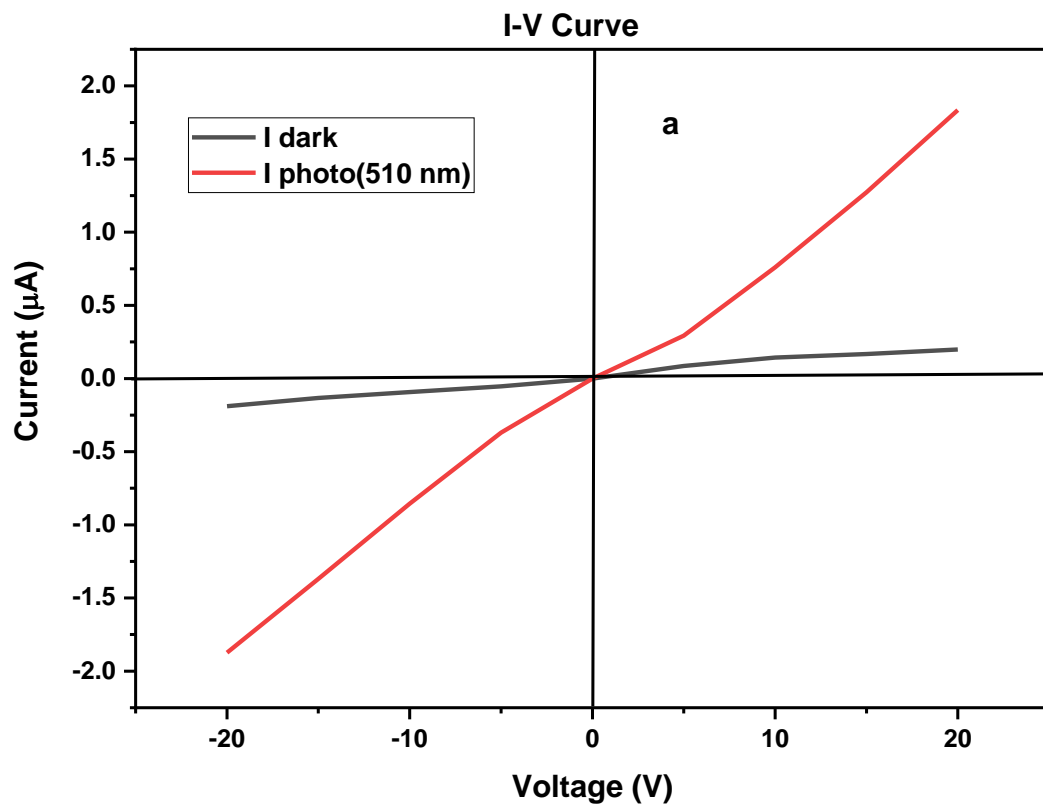
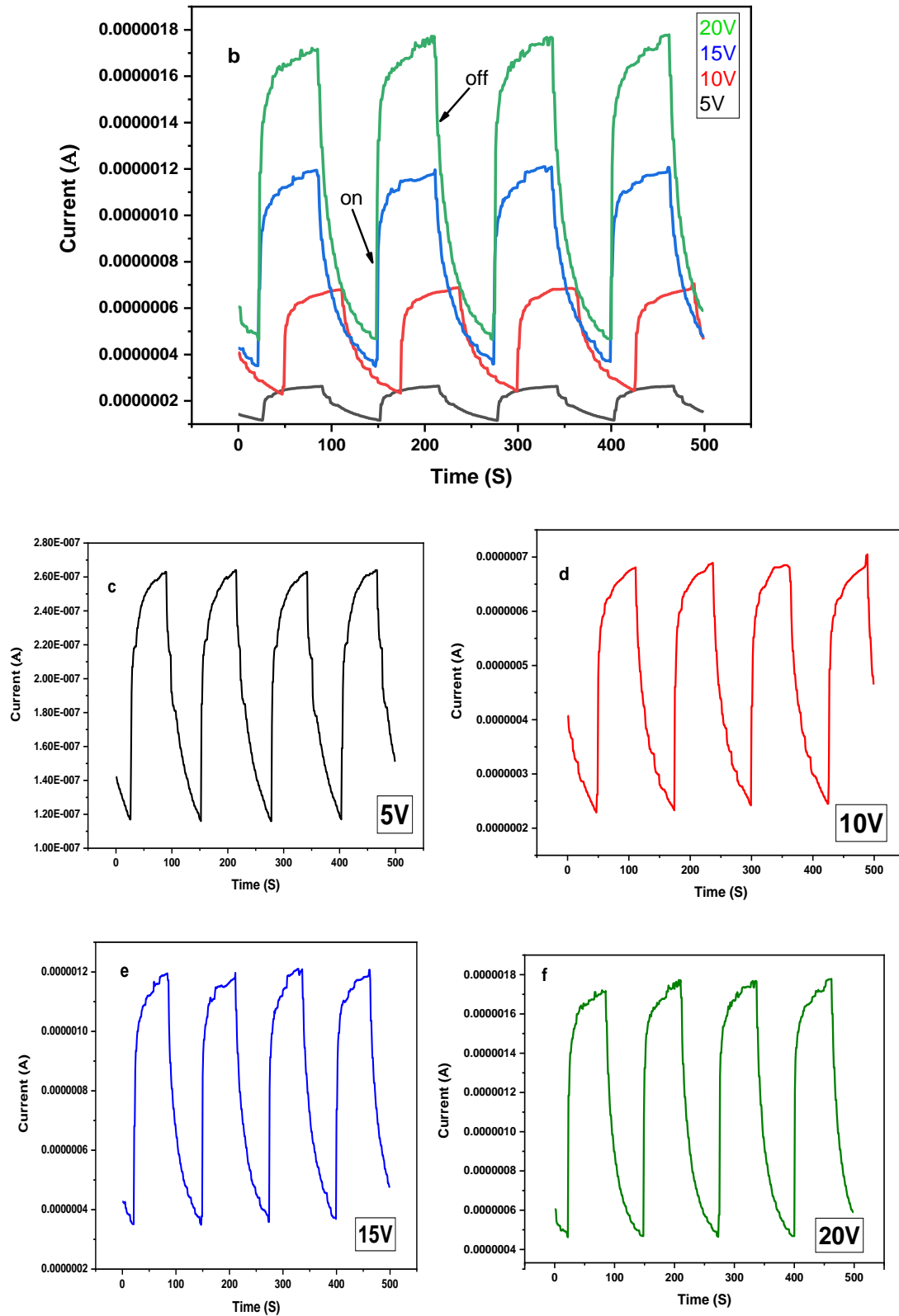


Figure 2: Shows (a) absorbance, (b) transmittance spectrum and (c) Energy gap of the  $\text{Fe(phen)}_2(\text{SCN})_2$  thin film.





**Figure 3:** Show (a) I-V characteristics in the dark and under visible illumination, (b) Photo-current response spectra at 510 nm wavelength at different bias voltage; and (c), (d), (e) and (f) Photo current response spectra at 510 nm wavelengths at 5 V, 10 V, 15, and 20 V respectively, of the Fe(phen)<sub>2</sub>(SCN)<sub>2</sub> photodetector.

**Table 1: Selection of Bragg peaks extracted from X-ray diffractograms.**

Complex thin film	Average crystallite size (XRD) (nm)	The diffraction peak position (2θ°)
Fe(phen) <sub>2</sub> (SCN) <sub>2</sub>	33.16	11.02, 17.55, 19.22, 21.40, 22.10, 23.82, 25.53, 38.83

**Table 2: Show the photo response parameters exposure to visible wavelength of the Fe(phen)<sub>2</sub>(SCN)<sub>2</sub> photo-detector.**

Bias voltage (V)	Wavelength (nm)	Response Time (S)	Recovery Time (S)	I photo (μA)	Current gain	S <sub>ph</sub> (%)	η(%)
5	510	24	45	0.2	3.4	58.45	3.55
10	510	22.77	38.3	0.61	5.31	76.82	10.63
15	510	22.73	41.8	1.1	7.62	84.9	19.03
20	510	14.5	34.5	1.63	9.22	87.83	28.17

#### 4. Conclusion

A flexible photodetector utilizing *Iron (phen)* material was successfully manufactured on a glass substrate. The experimental findings demonstrated excellent characteristics, including long-term stability, high sensitivity (87.83%), quantitative efficiency fairly acceptable (28.17%), and a substantial photocurrent response to 510 nm light. When a bias voltage of 20 V was applied, the photodetector exhibited a response time of 14.5 seconds and a quick recovery time of 34.5 seconds upon exposure to 510 nm light. These impressive results can be attributed to the material's advantageous properties, such as the spin crossover of *Iron (phen)* molecule and a well-formed crystal

structure. Overall, this study presents a promising approach to developing flexible photodetectors with exceptional performance capabilities.

There is no comparison with other research because the prepared compound is new and was prepared as a photodetector for the first time.

#### 5. References

- [1] LI, X., ZHANG, J., YUE, C., TANG, X., GAO, Z., JIANG, Y., ... & CHEN, H., "Large-area flexible Visible-Short wavelength Infrared Photodetection based on III-V compound semiconductor membrane photodetector with high performance," pp. 1–14, 2022.
- [2] H. Xiang, J. Cheng, X. Ma, X.

- Zhou, and J. J. Chroma, *Near-infrared phosphorescence: Materials and applications*, vol. 42, no. 14, 2013. doi: 10.1039/c3cs60029g.
- [3] N. Kaul, *Carbenes: The Gathering Photophysics of Transition Metal Carbene Complexes*. 2023.
- [4] Budziak-Wieczorek, I., Ślusarczyk, L., Myśliwa-Kurziel, B., Kurziel, M., Srebro-Hooper, M., Korona-Glowniak, I., ... & Matwijczuk, "Spectroscopic characterization and assessment of microbiological potential of 1,3,4-thiadiazole derivative showing ESIPT dual fluorescence enhanced by aggregation effects," *Sci. Rep.*, vol. 12, no. 1, pp. 1–19, 2022, doi: 10.1038/s41598-022-26690-1.
- [5] *J. Franklin Inst.*, vol. 46, no. 4, p. 280, 1848, doi: 10.1016/0016-0032(48)90480-3.
- [6] W. P. Lustig, S. Mukherjee, N. D. Rudd, A. V. Desai, J. Li, and S. K. Ghosh, "Metal-organic frameworks: Functional luminescent and photonic materials for sensing applications," *Chem. Soc. Rev.*, vol. 46, no. 11, pp. 3242–3285, 2017, doi: 10.1039/c6cs00930a.
- [7] X. D. Crystallography, "Making photoactive molecular-scale wires," pp. 1–23, 2016.
- [8] A. Pandikumar, S. Murugesan, and R. Ramaraj, "Functionalized silicate sol - Gel-supported TiO<sub>2</sub> - Au core - Shell nanomaterials and their photoelectrocatalytic activity," *ACS Appl. Mater. Interfaces*, vol. 2, no. 7, pp. 1912–1917, 2010, doi: 10.1021/am100242p.
- [9] W. Ouyang, F. Teng, J. H. He, and X. Fang, "Enhancing the Photoelectric Performance of Photodetectors Based on Metal Oxide Semiconductors by Charge-Carrier Engineering," *Adv. Funct. Mater.*, vol. 29, no. 9, pp. 1–20, 2019, doi: 10.1002/adfm.201807672.
- [10] Y. Su, Y. Zhang, C. Qiu, X. Guo, and L. Sun, "Silicon Photonic Platform for Passive Waveguide Devices: Materials, Fabrication, and Applications," *Adv. Mater. Technol.*, vol. 5, no. 8, pp. 1–19, 2020, doi: 10.1002/admt.201901153.
- [11] Huang, W., Xing, C., Wang, Y., Li, Z., Wu, L., Ma, D., ... & Zhang, H, "Facile fabrication and characterization of two-dimensional bismuth(iii) sulfide nanosheets for high-performance photodetector applications under ambient conditions," *Nanoscale*, vol. 10, no. 5, pp. 2404–2412, 2018, doi: 10.1039/c7nr09046c.
- [12] Chen, T. P., Wu, K., Li, Q., Chen, B., Kandel, H., Chen, J. C., ... & Al-Hilo, A., "2-D and mott transition studies on metal (M) doped PrBa<sub>2</sub>Cu<sub>3</sub>O<sub>7</sub>," *J. Low Temp. Phys.*, vol. 173, no. 3–4, pp. 89–105, 2013, doi: 10.1007/s10909-013-0893-7.
- [13] B. D. Vierzicke, S. Patel, B. E. Davis, and D. P. Birnie, "Evaluation of the Tauc method for optical absorption edge determination: ZnO thin films as a model system," *Phys. Status Solidi Basic Res.*, vol. 252, no. 8, pp. 1700–1710, 2015, doi: 10.1002/pssb.201552007.
- [14] H. M. Jabbar, "Optical

- Properties of vanadium pentoxide prepared by sol gel method,” *J. Kufa-Physics*, vol. 10, no. 01, 2018.
- [15] H. B. Tarikhum, F. Almyahi, and B. Ali, “Optical, Structural, and Electrochemical Properties of P3HT:Y6 Photoactive Layer for Organic Photovoltaics,” *Karbala Int. J. Mod. Sci.*, vol. 9, no. 4, pp. 618–627, 2023, doi: 10.33640/2405-609X.3328.
- [16] H. M. Jabbar, E. M. Jaboori, and A. Q. Abdullah, “Dispersion parameters, optical constant and photoluminescence of poly vinyl alcohol grafted eosin-Y dye (PVA-g-Ei),” *J. Basrah Res.(Sci.)*, vol. 36, pp. 9–16, 2010.
- [17] Sebastian, S., Vinoth, S., Prasad, K. H., Revathy, M. S., Gobalakrishnan, S., Praseetha, P. K., ... & AlFaify, S. “Quantitative analysis of Ag-doped SnS thin films for solar cell applications,” *Appl. Phys. A Mater. Sci. Process.*, vol. 126, no. 10, 2020, doi: 10.1007/s00339-020-03959-8.
- [18] D. S. Drozd, “PHOTOELECTRONIC PROPERTIES OF CDSE AND CDTE NANOWIRES,” no. December, 2010.
- [19] F. H. Alsultany, Z. Hassan, and N. M. Ahmed, “A high-sensitivity, fast-response, rapid-recovery UV photodetector fabricated based on catalyst-free growth of ZnO nanowire networks on glass substrate,” *Opt. Mater. (Amst.)*, vol. 60, pp. 30–37, 2016, doi: 10.1016/j.optmat.2016.07.004.
- [20] P. Royo, R. P. Stanley, M. Ilegems, K. Streubel, and K. H. Gulden, “Experimental determination of the internal quantum efficiency of AlGaInP microcavity light-emitting diodes,” *J. Appl. Phys.*, vol. 91, no. 5, pp. 2563–2568, 2002, doi: 10.1063/1.1433938.
- [21] F. A. Kasim, M. A. Mahdi, J. J. Hassan, and S. J. Kasim, “Preparation and optical properties of CdS / Epoxy nanocomposites,” vol. 5, pp. 57–66, 2012.